Post-irradiation microstructural examination of EUROFER-ODS steel irradiated at 300°C and 400°C

M. Klimenkov[*1], U. Jäntsch[1], M. Rieth[1], M. Dürrschnabel[1], A. Möslang[1], H.-C. Schneider[2]

[1]Karlsruhe Institute of Technology, Institute for Applied Materials (IAM-AWP), Eggenstein-Leopoldshafen, Germany

[2]Karlsruhe Institute of Technology, Institute for Applied Materials (IAM-WBM), Eggenstein-Leopoldshafen, Germany

Abstract:

The effect of neutron irradiation on the microstructure of EUROFER-ODS alloy reinforced with an addition of 0.5% Y_2O_3 was analyzed by transmission electron microscopy. The irradiation of up to 16.2 dpa damage dose at 300°C and 400°C was performed in Petten High Flux Reactor. This study focuses on the imaging, identification, and quantitative analysis of interstitial loops and voids located on ODS particles. The nano-sized loops and point defects with b½⟨111⟩ Burgers vectors are preferentially located near structural defects such as the line dislocations or impurities in the material irradiated at 300°C. Homogeneously distributed loops having Burgers vectors of type b½⟨111⟩ and b⟨100⟩ were found in the material irradiated at 400°C. The obtained quantitative data on radiation-induced defects such as size, number density and relaxation volume were compared with EUROFER97 irradiated at the same conditions. It was found that the occurrence of radiation induced defects depends on the local number density and the size distribution of the ODS particles and not only on the irradiation damage and temperature.

Corresponding author: Michael Klimenkov
Institute for Applied Materials (IAM)
Karlsruhe Institute of Technology
Hermann-von-Helmholtz-Platz 1
76344 Eggenstein-Leopoldshafen, Germany

Phone: +49 721 608 2 2903
Fax: +49 721 608 2 4567
email: michael.klimenkov@kit.edu

1. Introduction:

Ferritic-martensitic oxide-dispersion-strengthened (ODS) steels are promising candidates for numerous applications in nuclear and fusion technology due to their superior radiation resistance properties [1,2]. The importance of this topic is shown by the fact that dozens of ODS alloys have been developed, optimized and tested over the last two decades, and yet this has not lost any of its relevance [3–5]. The most recent development focus on the production and characterization of austenitic ODS alloys [6]. An ODS variant of EUROFER97 was developed with the purpose of further increasing the operating temperature and thus the efficiency of advanced blanket concepts for fusion reactors.

Neutron irradiation and ion implantation are both experimental techniques applied for the verification of radiation resistance of ODS steels [4,7–9]. The advantages of ion implantation are relatively low costs, short irradiation time, providing non-radioactive samples [4,9,10] as well as the ability to accumulate significant damage of several tens of dpa in the acceptable time scale [5]. However, the influence of ion and neutron irradiation on the microstructure can be quite different, since the damage rate appears as an important factor for defect formation [11]. For this reason, the study of microstructure of neutron irradiated ODS alloys is of great importance to understand their structural evolution under application conditions. It should be mentioned that enormous technical efforts and costs for neutron irradiation experiments make the published work on neutron irradiation of ODS materials quite rare [8,12].

As neutron irradiated EUROFER-ODS steels show in a wide temperature window superior tensile and fatigue properties compared to casted steels like for example EUROFER 97 [13], the knowledge of the defect formation mechanisms is important to understand the effect of ODS particles on radiation resistance and the relationship between irradiation modified microstructures and mechanical properties. Highly dispersed oxide particles serve as trapping sites for vacancies and self-interstitial atoms, preventing the formation and coarsening of radiation-induced defects that lead to degradation of mechanical properties. Most studies of irradiated ODS materials are focused on demonstrating the stability of ODS particles [7,14,15] and to a lesser extent, on the formation of radiation-induced defect [8,16]. Our work intends to fill the current knowledge gap and contribute to a better understanding of the radiation resistance mechanism of ODS alloys.

The experimental results of this study reveal the microstructural properties of radiation-induced defects formed at 300°C and 400°C. These should complete the characterization of the of the first generation EUROFER97 and EUROFER-ODS alloys irradiated within the SPICE

program, which are already published earlier [3,12]. In addition to a detailed defect analysis, it is also shown that the formation of radiation-induced defects depends not only on the irradiation temperature but also on the local distribution of ODS particles (i.e., size and local number density). The temperature influence on the formation of radiation-induced defects will be discussed with a regard to these previously published results.

2. **Experimental:**

The EUROFER-ODS alloy examined in this study was fabricated by mechanical alloying of EUROFER97 powder with addition of 0.5 wt% Y_2O_3 in industrial ball mills the type attritor (Plansee, Austria). The EUROFER97 powder of 8.9 wt% Cr, 1.1 wt% W, 0.2 wt% V, 0.14 wt% Ta, 0.42 wt% Mn, 0.06 wt% Si, 0.11 wt% C composition was produced by inert gas atomisation (HC-Starck, Laufenburg, Germany). Hot Isostatic Pressing (HIP) was used as a consolidation process for the production of bars with a diameter of 60 mm and a length of 300 mm. This material was available for numerous laboratories in Europe and has been comprehensively characterized [17]. The tensile and Charpy specimens for irradiation program were prepared from the hipped material without further thermal treatment. The neutron irradiation was carried out in the Petten High Flux Reactor (HFR) within the framework of the HFR irradiation project Phase IIb (SPICE) with a nominal dose of 16.3±1.9 dpa at the targeted irradiation temperatures of 250°C, 300°C, 350°C, 400°C and 450 °C. [18]. The content of transmutation-induced helium was estimated to <10 appm. The present work reports the microstructure of EUROFER-ODS irradiated at 300°C and 400°C targeted temperature. The average temperature measured during irradiation was (293±8)°C and (392±8)°C, accordingly. Since the target and average temperatures are within the error range, we use the target temperature when discussing the results. The microstructure of the material irradiated at 250°C, 350°C and 450°C targeted temperatures was investigated and published by Klimenkov et al. [12].

The TEM specimens were prepared by electrochemical etching. Disks with a thickness of 0.2 to 0.3 mm and 3 mm in diameter were thinned by electropolishing in a TENUPOL V device using H_2SO_4 + 80 % CH_3OH electrolyte. In the next step, disks of 1 mm diameter were punched with the hole in the middle to minimize the quantity of the radioactive sample and thus the irradiation exposure and optical distortion caused by the magnetic field in TEM. TEM investigations were performed using a FEI Tecnai 20 FEG analytical microscope with an accelerating voltage of 200 kV. Preparation and analysis of the irradiated samples was done in the controlled area of the Fusion Materials Lab at KIT.

The Burgers vector of dislocation loops was determined by weak beam dark field (WBDF) imaging with low indexed **g**(n**g**) vectors near the [100] and [111] zone axes. The tilt experiments were performed using a standard FEI double tilt holder. The corresponding visibility criteria of the dislocation loops for different *g*-vectors are listed in tables 1 and 2.

g \ ***b***	½[111]	½[$\bar{1}$11]	½[1$\bar{1}$1]	½[11$\bar{1}$]	[001]	[010]	[100]
[$\bar{1}$10]	0	1	0	0	0	1	1
[$\bar{1}$01]	0	1	1	1	1	0	1
[01$\bar{1}$]	0	0	1	1	1	1	0
[020]	1	1	1	1	0	2	0

Table. 1 |b·g| values for [111] beam direction and for ***g***=[020] near [102] zone axis.

g \ ***b***	½[111]	½[$\bar{1}$11]	½[1$\bar{1}$1]	½[11$\bar{1}$]	[001]	[010]	[100]
[011]	1	1	0	0	1	1	0
[01$\bar{1}$]	0	0	1	1	1	1	0
[002]	1	1	1	1	2	0	0
[020]	1	1	1	1	0	2	0
color	blue	blue	red	red	yellow	green	------

Table. 2 |b·g| values for all **g** vectors in orientations close to the [100] zone axis. The loops of defined Burges vector are drawn with corresponding colours in the Figs. 7 and 8.

3. **Results**

3.1 Microstructure of unirradiated material

The EUROFER-ODS alloys with 0.3 % and 0.5 % Y_2O_3 has been subjected to an extensive examination in the past [12,19–21]. Their microstructure consists of ferritic grains with an average size of several micrometers [12]. The presence of two types of precipitates has been reported: Micrometer-sized $(Cr,Fe)_{23}C_6$ carbides, located mostly at the grain boundaries, and finely dispersed nanometer-sized ODS particles, composed basically of Y_2O_3 [12,19]. In general, the grain structure and distribution of ODS particles of the alloy with 0.5% Y_2O_3 are very similar to that of the EUROFER-ODS alloy containing 0.35% Y_2O_3 [20,21]. Despite this

comprehensive knowledge, we present new aspects of the composition of ODS particles that have not been published previously.

Analytical investigations demonstrating spatial distribution of ODS particles in both areas are shown in Fig. 1. The HAADF image of investigated area is given in Fig. 1a, while the elemental maps using Y-L and Ta-M, V-K and Fe-K EDX lines of the marked area are presented in the parts (b)-(e) respectively. The size distribution of the ODS particles shows significant variations for different areas. In the "coarse" area, the size of ODS particles varied from 5 nm to 25 nm with number density that varied for different locations from $2.5*10^{20}m^{-3}$ to $5.0*10^{21}m^{-3}$ (Fig. 1 left side). The "fine area" shows a quite homogeneous distribution of particles with sizes smaller than 5 nm. (Fig. 1b right side). The number density there was measured to $(1.5\pm1.0)*10^{23}$ m^{-3} (up to ~100 times higher than in the “coarse area”). The thickness of the TEM film in the investigated area was measured using electron energy loss spectroscopy. The analysis of several TEM images show that about 2/3 of the material consists of the "fine" area and about 1/3 of the "coarse" area. The appearance of the these two areas follows to a random pattern that does not reflect the grain structure of the material. It can be assumed that the areas with different

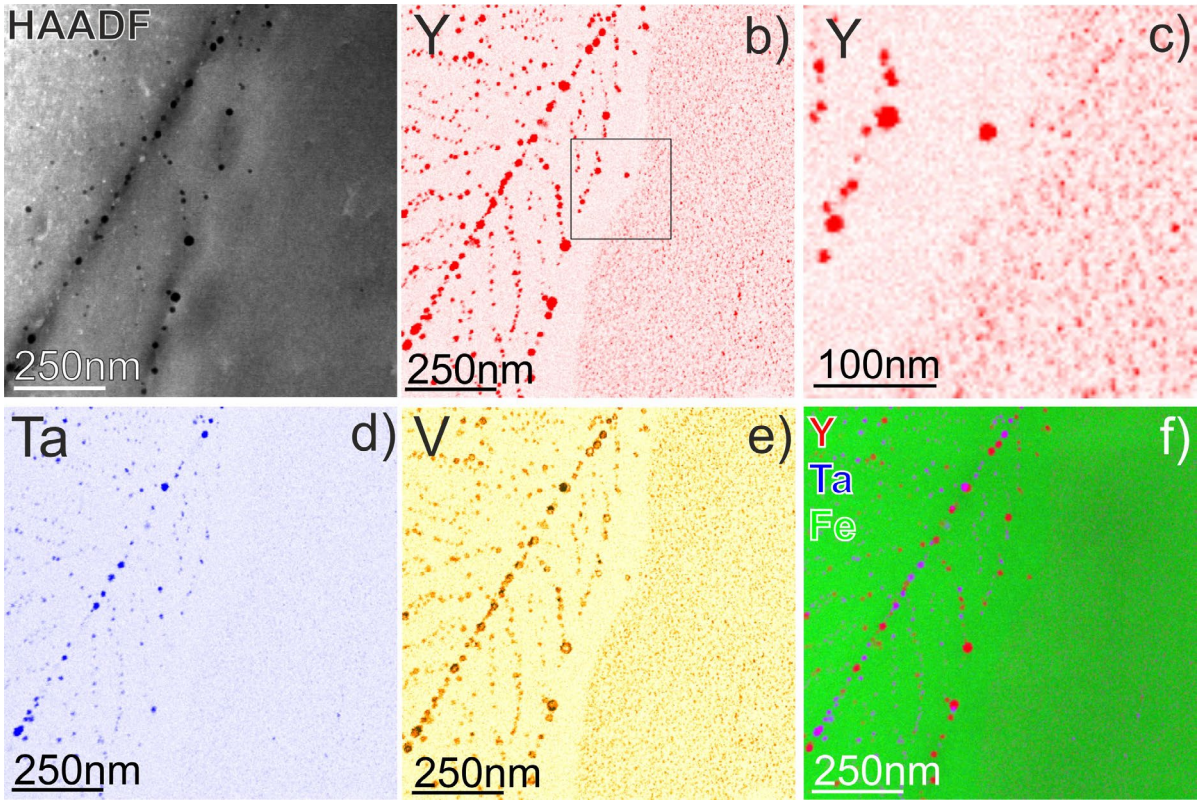

Fig. 1 Analytical examination of unirradiated EUROFER-ODS. The HAADF image of analyzed area is shown in part (a) and the maps of the corresponding elements imaged with reverse contrast are shown in parts (b-e). Part (c) shows an enlarged section from part (b) which is marked with a square. The part (f) represents composition of Y (red), Ta (blue) and Fe (green) maps.

distribution were formed as a result of Y_2O_3 distribution on powder particles during mechanical alloying.

The different nomenclatures were proposed by B. Odette [22] to distinguish between nanostructured ferritic alloys (NFAs) and oxide dispersion strengthened (ODS) steels. The main criterion for this distinguishing is the size distribution and number density of the oxide particles. Accordingly, the 10-15 nm oxide particles as found for example in PM2000 steel [23] are called as “ODS particles” and finely dispersed oxides of a few nanometers in size and number density $>10^{23}$ m^{-3} are called nano oxides (NO). Since both types of particles are present in the EUROFER-ODS alloy, the particles in the coarse region are referred to as “ODS particles” and the particles in the fine region are referred to as NO.

The existence of areas with different distribution of ODS particles, known as "bimodal distribution", was already reported in a previous work [12,24,25]. Often, a bimodal distribution is associated with changes in grain size, where the "coarse area" is located in the grains smaller than 70 nm, while the formation of nano oxides in the "fine area" was observed in the large grains of 2-3 μm size [25]. Due to the significant influence of ODS particles distribution on the formation of radiation-induced defects, these two different areas will be referred to as "coarse area" and "fine area" in the following [12].

The large scale analysis of ODS particles showed that, depending on the position, 5% to 25% of the ODS particles in the "coarse" region have a (Ta,V,Y)O composition (Fig. 1c), while no such particles were observed in the fine region. This phase occurs as a separate particle or as a core in a complex particle typically surrounded by the Y_2O_3 phase. The (Ta,V,Y)O particles have a spherical shape very similar to that of Y2O3 particles, hence their identification on the basis of bright-field TEM images is practically impossible. The presence of Ta-rich oxide particles is the only visible difference between the coarse and the fine areas, suggesting that it may have played a role in the formation of the bimodal distribution. It can be assumed that based on the core-shell structure of some particles with (Ta,V,Y)O core and Y_2O_3 shell that the precipitation of the Ta-rich phase occurs on the earlier stages of hot isostatic pressing than that of Y_2O_3 particles. This initial formation of nucleation centers could promote the formation of ODS particles with sizes up to 30 nm. This is only an assumption, because so far there is no generally recognized explanation in the scientific literature for the bimodal size distribution of ODS particles in the same material class.

To the best of our knowledge, the formation of Ta-rich ODS particles has not been previously reported, despite an extensive characterization of the EUROFER-ODS alloy over 2 decades.

The reasons for this are presumably the similar morphology for the one and nearly overlapping of Ta-Mα,β (1.73-1.81keV) with W-Mα,β (1.77-1.83keV) and Y-Lα (1.92keV) EDX lines. The separation of Y and Ta was clearly possible by using the Ta-Lα (8.1keV) and Y-Kα (14.93keV) lines for the detection. The V-rich phase occurs in both areas. In the coarse area, it occurs as a shell around ODS particles and as nano-sized “eyes” on ODS particles (Fig. 1d). It is reasonable to assume that a thin V-rich layer has also formed around nano oxides in the "fine" area, however, clear imaging of such closely spaced, nano-sized, structures is below the sensitivity of analytical transmission electron microscopy.

3.2 **Investigation of material irradiated at 300°C**

The microstructure of the sample irradiated at 300°C is shown in Figs. 2-5. Fig. 2 marks the differences in defects formation inside “fine” and “coarse” areas. The WBDF image acquired using g = [020] shows the defects in a grain oriented close to the [102] zone-axis (Fig. 2a). The Y- and Cr-EDX maps visualize the distribution of ODS particles and $M_{23}C_6$ precipitates and allow an exact location of these both areas (Fig. 2b,c). The areas have the same crystallographic orientation and are thus parts of the same grain. This can be concluded from their identical g -

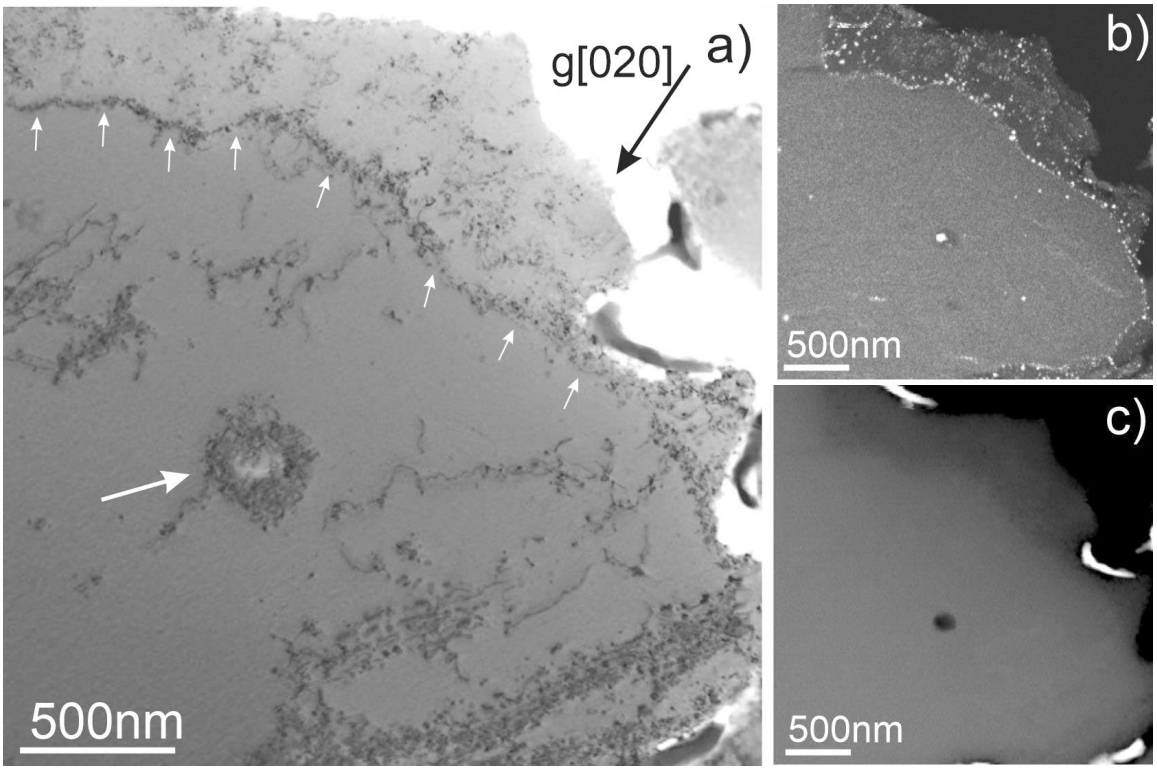

Fig. 2 Microstructure of EUROFER-ODS irradiated at 300°C. a) WBDF image with reversed contrast using the g[020] reflection. The Y map (b) and Cr (c) maps indicate the location of the “fine” and “coarse” areas as well as $M_{23}C_6$ precipitates.

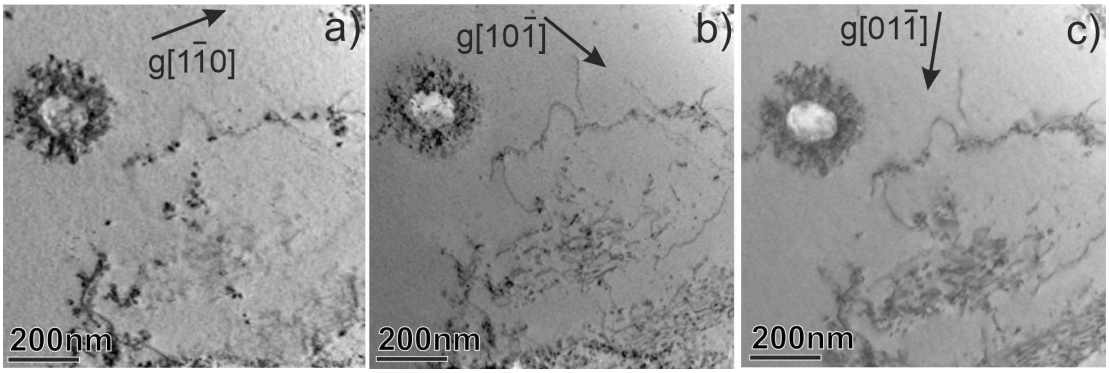

Fig. 3 The micrographs of the "fine" area obtained at WBDF conditions with selected ***g***-vectors near the [111] ZA and imaged with reversed contrast.

conditions for all orientations. The "fine" area with one large Y_2O_3 particle (marked with the white arrow) is located in the center of the image, while the "coarse" area is located in its upper part (Fig. 2b). An average line dislocation density of $(1.3\pm0.6)*10^{13}m^{-2}$ and $(7\pm4)*10^{13}m^{-2}$ was measured for the "fine" and "coarse" areas, respectively. However, there are variations in dislocation density by a factor of 2-5 for different grains.

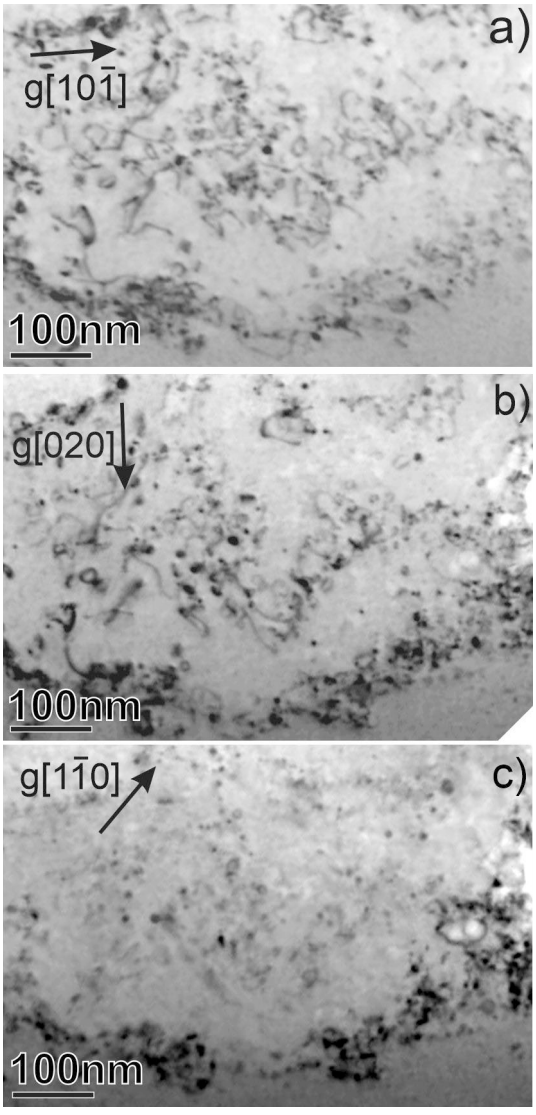

Fig. 4 The micrographs of the "coarse area" obtained at WBDF conditions with selected ***g***-vectors near [111] zone-axis and imaged with reversed contrast.

The Burges vector of the radiation-induced defects and line dislocations was determined by the orientation of the grain near the [111] and [102] zone-axis as shown in Fig. 3 and Fig. 4. The *g*-vectors used for this purpose are listed in Tab. 1. Since the imaging with g-vectors of ⟨110⟩ type near [111] zone axis does not allow a unambiguous determination of the Burgers vector for all defects, the sample was tilted to the zone-axis and imaged with **g**[002] (Fig. 2a). It should be pointed out that all defects indicate the same direction of the Burger vector - b½[11-1] over wide areas,

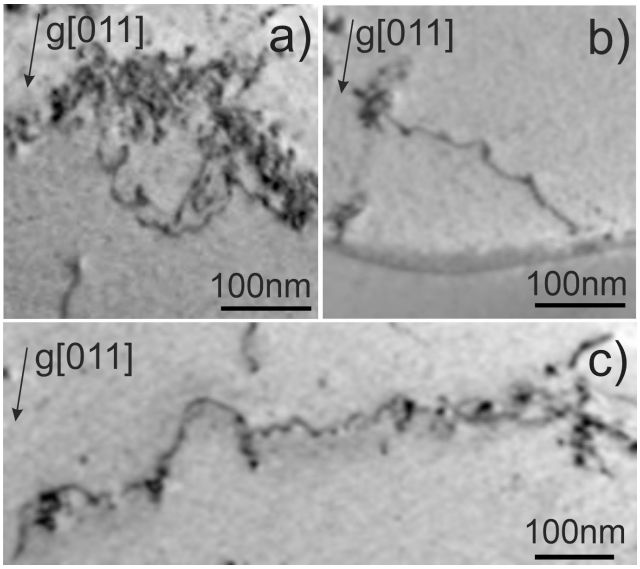

Fig. 5 Formation of helical dislocations in the “fine area”.

since 90% of them are invisible in the g[1-10] images (Figs. 3c and Fig. 4c). Examination of several grains suggests that this preferential orientation of the Burger vector is frequently present in irradiated EUROFER-ODS steels.

The loops or point defects observed in the "fine" area tend to be adjacent to structural defects such as line dislocations, single Y_2O_3 particles (Fig. 2. 3), or grains between "coarse" and "fine" areas (Fig. 2a – marked with white arrows). A high density of radiation-induced defects, as visible for example in the lower part in Fig. 3, is the result of the higher local density of line dislocations. In contrast, the dislocation loops in the "coarse" area show a homogeneous spatial distribution (Fig. 4). The detailed quantitative analysis of size and number density of radiation induced defects for both areas are shown in the discussion section.

It was found that a single, separately located ODS particle (marked by arrow in Fig. 1a) can be found randomly in the fine area sounded by nano oxides. The dislocation loops, as shown in Fig. 3, are also preferentially located close such to single ODS particle. They mainly have a Burgers vector of the ½⟨111⟩ type. The analysis of each loop proved impossible due to its high local density. A similar clustering of defects around ODS particles was also observed in neutron-irradiated EUROFER-ODS after irradiation at 250° [12].

Analyses of the acquired TEM images reveal that several line dislocations in the "fine" area have a tendency to transform into a helical dislocation. Fig. 5 presents several examples where the initial stage of its formation could be observed. The periodicity of the helix varied from 30 nm to 60 nm and its diameter from 5 nm to 15 nm. The maximal diameter of the helix observed in this study is about 30 nm (Fig. 4a).

The nano-sized voids or bubbles located on the ODS particles were observed in the "coarse" area. However, their appearance is irregular, so we excluded the voids from the detailed statistical analysis. The number density and size of the voids shown in Tab. 3 are a rough estimate based on analysis of several TEM micrographs.

3.3 **Investigation of material irradiated at 400°C**

Both dislocation loops and voids located on ODS particles were detected in the material irradiated at 400°C. The voids were formed only in the "coarse" area and only at the ODS particles, as shown for example in Fig. 6a (marked by arrows). We have found no evidence for their existence in the "fine" area, but we cannot completely exclude it, since nanoscale (~1 nm) voids cannot be clearly distinguished from nano oxides. Their occurrence is not homogeneous i.e., in some "coarse" areas voids were found on each ODS particle, in some other areas with ODS particles no voids were found.

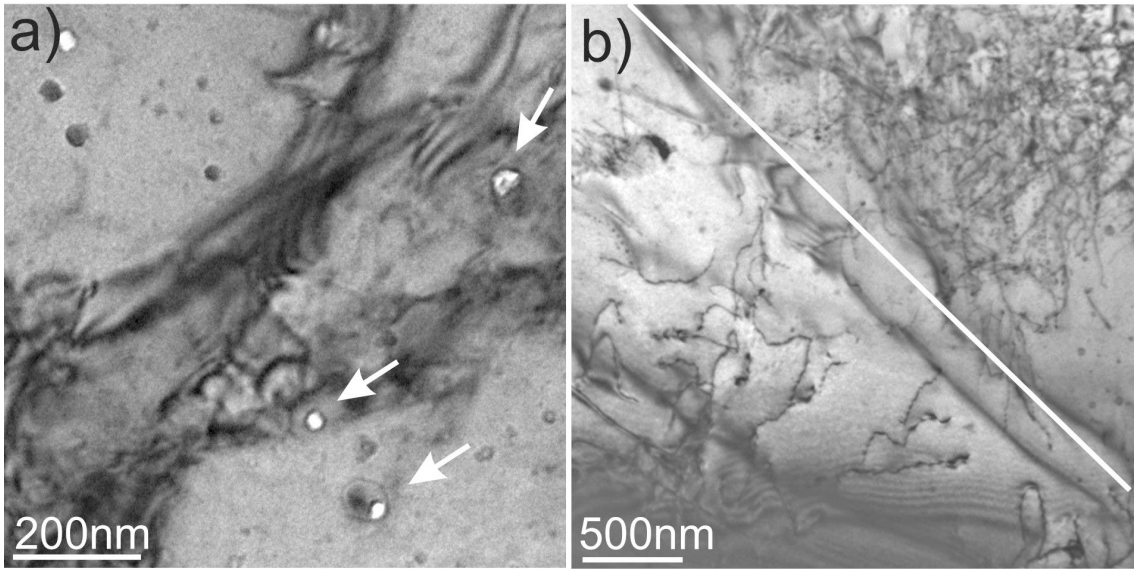

Fig. 6 The BF image of ODS particles with voids (a) and BF image illustrating the distribution of dislocations in the “coarse” (right side) and “fine” (left side) areas (b).

The BF image in Fig. 6b illustrates typical microstructural differences between "fine" (bottom left side) and "coarse" (upper right side) areas, with the white line indicating approximately the boundary between them. The density of line dislocations was determined as $(4\pm1.5)*10^{13}m^{-2}$ in the "fine" and as $(1.6\pm0.7)*10^{14}m^{-2}$ in the “coarse” area (see Tab. 3). Analyses of several grains show that the “coarse” areas have a systematically 3-5 times increased dislocation density compared to the “fine” areas. In the "coarse" area, the formation of b<100> dislocation junctions formed by the interaction of two b½<111> non-coplanar line dislocations have often been observed. Since the junctions with b<100> were typically detected in the plastically deformed material [26], their occurrence in the "coarse" area could be considered as an indication of a radiation-induced movement of the line dislocations. The fact that in unirradiated EUROFER-ODS no junctions were observed additionally confirms this assumption.

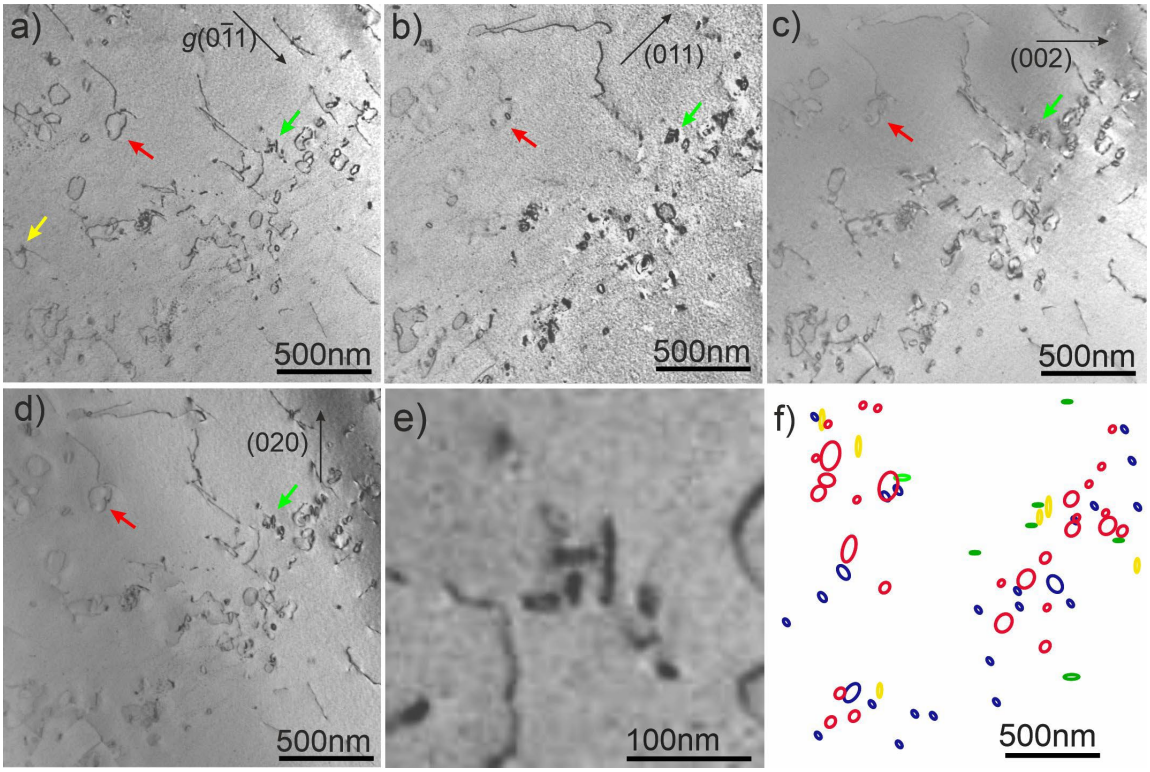

Fig. 7 The micrographs obtained at WBDF conditions with selected ***g***-vectors near [100] ZA (parts a-d). The part (e) shows the presence of b<100> loops. In part (f), loops with b[1-11] and b[111] Burgers vectors are schematically drawn with red and blue colors, and b[010] and b[001] loops are drawn with green and yellow colors, respectively.

Due to the high dislocation density in the coarse areas, we omitted a detailed statistical evaluation of the dislocation loops there. It was observed that the larger loops were often cut off by the foil surface. Such loops are often visible as typical line dislocations [3]. This effect also leads to a significant distortion of the loop statistics.

The WBDF imaging with different g-vectors near the [100] zone-axis was applied to determine the Burgers vector of dislocation loops (Fig. 7). In the parts (a)-(d) are shown two beam images with all four low indexed g-vectors. The Burgers vector of the loops were identified based on their projections and visible criteria. The 90% of loops have a b½<111> Burgers vector, while only a few b<100> loops were observed. The accumulation of b<100> loops is indicated by a green arrow in g-images and displayed enlarged in Fig. 7e. The b<100> loops are frequently found as individual loops, so that such "agglomerations" of 5 loops in a limited space are rather exceptional. The maximum size of the b<100> loops is about 30 nm, which is considerably smaller than for the b½<111> loops, whose size can exceed 120 nm. Fig. 7f summarizes the results of Burgers vector analysis, where the loops are imaged using different colors according to their respective Burgers vector.

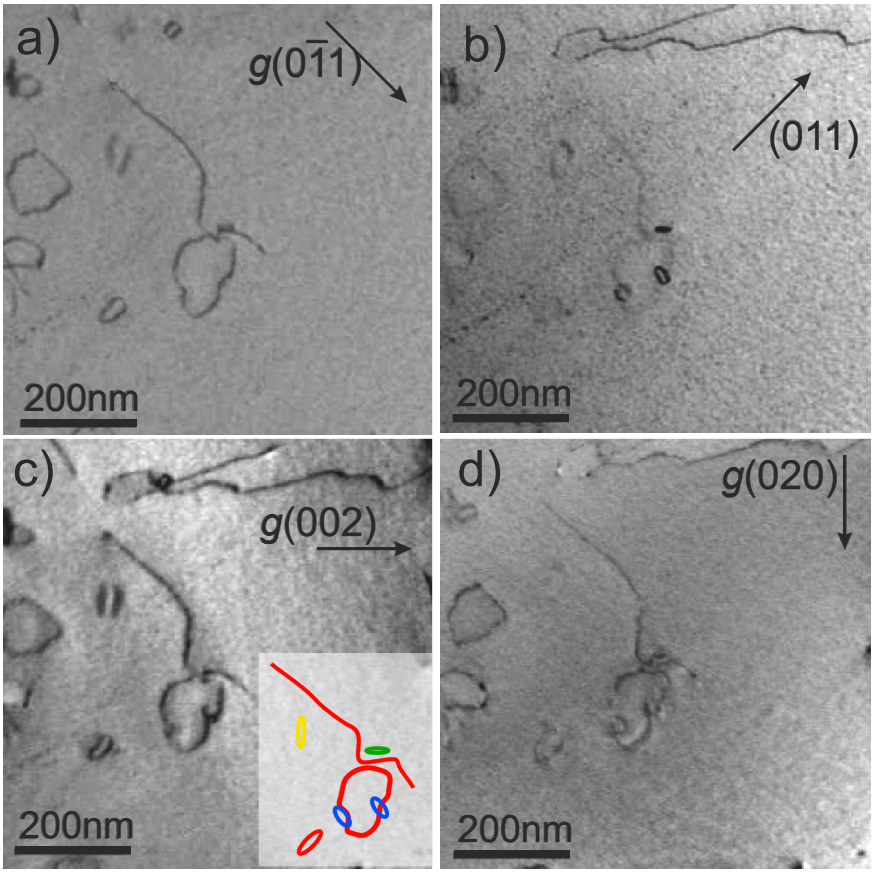

Fig. 8 The interaction of b½<111> loops imaged with different g-vectors near the [100] zone axis. The loops are drawn in part (c) with colors according to Tab. 2: b½[1-11] red, b½[111] blue, b[002] yellow and b[020] green.

Despite the low number density of $4.5*10^{20}$ m^{-3}, the loops often interact with each other and with the line dislocations. Examples of such interactions are shown in Figs. 8 and 9. Fig. 8 presents a detailed analysis of interacting b½<111> loops with different Burgers vector directions. The 150 nm sized loop with b½[1-11] (red color) interacts with two 20 nm sized loops having a b½[111] Burgers vector (blue color). The colors used for the labeling the Burgers vector were selected according to Tab. 2. The shape of the large loops shows a deformation at the points where it touches the smaller loops (Fig. 8a). The invisibility of the contact position in Fig. 9d indicates the formation of a junction having a b[001] Burgers vector.

Fig. 9 shows the interaction of the line dislocation with a loop, where the line dislocation has a characteristic bow. Such structures are frequently observed in the sample. Both the bow and the line dislocation have the same Burgers vector of type b½<111> and the same direction. It can be assumed that the line dislocation moves in the habitat plane of the dislocation loops and causes an annihilation of the loops. This process explains the low number density of dislocation loops of $4.5*10^{20}m^{-3}$ being present in this area.

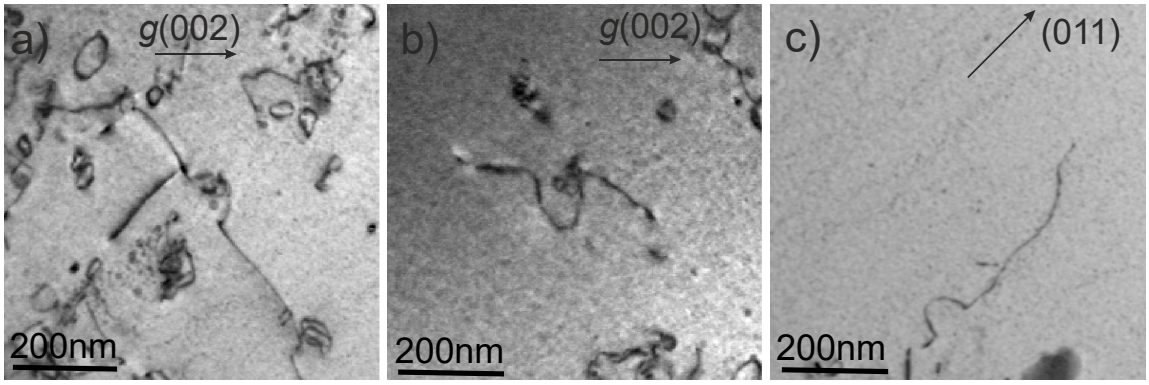

Fig. 9 The micrographs show a possible interaction of line dislocations with dislocation loops.

4. **Discussion**

The microstructural response of different ODS-based alloys to neutron or ion irradiation has been extensively studied in the past using TEM or atom probe tomography (APT) methods [12,27,28]. Typically, the microstructural examination of ODS materials focused on the radiation effect on the size, distribution, and chemical composition of ODS particles [11]. The formation of radiation-induced defects such as loops or voids in ODS materials has rarely been the subject of research. The formation of small point defects, "black dots", was analyzed for example in neutron irradiated EUROFER-ODS alloys up to a dose of 3 dpa at 300°C, 450°C and 550°C [8]. At present time, 300°C is the lowest irradiation temperature for ODS steels being reported in scientific literature. The stability of ODS particles under neutron irradiation and the low formation threshold for dislocation structures have been reported for irradiation temperatures above 400°C [8,29]. This limited amount of published data and the unequal

T_{irr}	area	density of line dislocations /$\times 10^{13}$ m^{-2}	loop number density /$\times 10^{21}$ m^{-3}	average size /nm	void number density /$\times 10^{19}$ m^{-3}	void swelling %	relaxation volume /%	fraction of ½⟨111⟩ loops
300°C	fine	1.3±0.6	1.0±0.7	7	---------	------	0.008±0.005	100%
	coarse	7±4	5.0±1.5	13	0.5±0.4	~0.004	0.035±0.015	95%
400°C	fine	4.0±1.5	0.45±0.20	71	---------	---------	0.035±0.02	90%
	coarse	17±8	1.0±0.5	94	3.0±2.0	~0.02	0.08±0.03	85%

Tab. 3 Quantitative and statistical data of dislocation loops and voids obtained separately for "fine" and "coarse" areas.

irradiation conditions make a direct comparison of our own results with the scientific literature at least difficult or even impossible.

Tab. 3 summarizes all relevant statistical and quantitative data on dislocation loops and voids extracted by analyzing, among others, the demonstrated TEM images. The data includes average size, number density, Burgers vector, fraction of $\boldsymbol{b}$½⟨111⟩ loops and relaxation volume. The total number density of radiation-induced defects was obtained by taking into account that part of the defects is invisible at defined $\boldsymbol{g}$-conditions (Tab. 1,2). In the images with $\boldsymbol{g}$⟨200⟩, 100% of $\boldsymbol{b}$½⟨111⟩ loops and only 1/3 of $\boldsymbol{b}$⟨100⟩ loops are visible. Correspondingly, 50% of $\boldsymbol{b}$½⟨111⟩ loops and 66% of $\boldsymbol{b}$⟨001⟩ loops are visible in the images with $\boldsymbol{g}$⟨011⟩. The average of different g-images from several grains was determined as the total number density value of dislocation loops.

As shown in several publications, the ODS particles serve as a sink for vacancies or dissolved gas atoms, leading to the formation of bubbles/cavities directly on the particle surfaces, and thus preventing their influence on the mechanical properties [10,12,30,31]. Experimentally, this fact was confirmed in both ion and neutron irradiated ODS alloys. In the present study, the voids located on the ODS particles were formed only in the coarse area at both irradiation temperatures (Fig. 6). However, their appearance is irregular, so that a number density of ~$10^{19}$$m^{-3}$ was estimated with considerable error of 70%-90% (Tab. 3). The reasons for this are the irregular void formation and the estimation of the occurrence of the "fine" and "coarse" areas. The existence of nanometer-sized voids in the "fine" area cannot be definitely excluded, since they would be indistinguishable from nano oxides in TEM images. Since no voids were found in the fine area after irradiation at 250°C, 350°C and 450°C, it can be assumed that the presence of nano oxides effectively prevents (or at least minimizes) their formation in a broad temperature range [12].

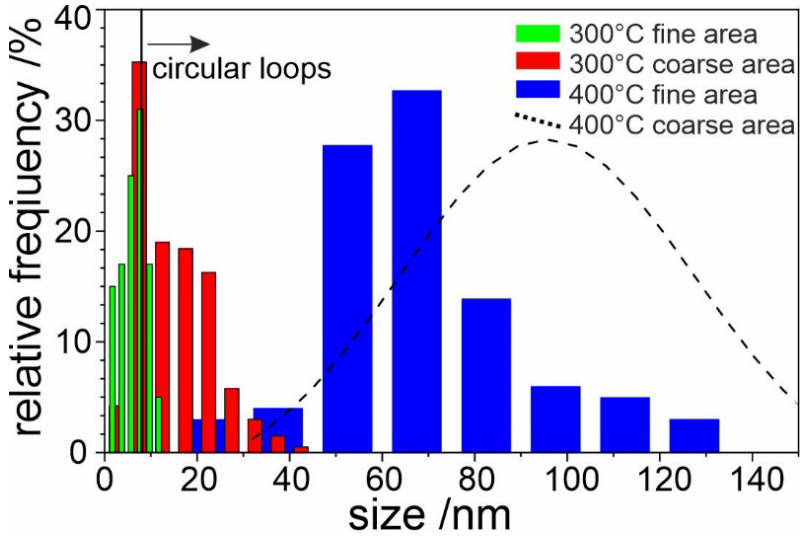

Fig. 10 Size distribution histograms of dislocation loops for 300°C and 400°C irradiation temperatures.

Radiation-induced formation of voids in ferritic-martensitic steels, including ODS alloys has typically been observed after neutron irradiation in a narrow temperature range from 300°C to 450°C [2,3,32]. It was also shown that the effect of neutron irradiation on microstructure is strongest in this particular temperature range. The presence of He or H in the matrix plays an important role in the void formation process i.e., it increases the void swelling by 3-5 times [31,32].

The size distribution histograms of the dislocation loops in both specimens are displayed in different colors in Fig 10. The radiation-induced defects formed at 300°C in the “fine area” show a narrow size distribution with sizes of less than 10 nm (green bars). The majority of them are referred to as "black dots", which have sizes less than ~7 nm. In the TEM images such loops show a dot-like projection without a recognizable structure, whereas the larger loops usually show a circular structure in the images. The separation line located at 7 nm in the diagram shows approximately the difference between "black dots" and clearly visible circular loops. In general, the size at which the loops are imaged as rings depends strongly on the sample thickness, alignment and indexing of the ***g***-vector and other imaging conditions. The loops in the coarse area show a broad distribution with sizes up to 30 nm and a significantly higher number density.

The loops formed at 400°C in the “fine” area show a broad size distribution ranging from 20 nm to 130 nm with an average value of 65 nm. The distribution in the "coarse" area has been roughly estimated and drawn using a dashed line instead of a bar histogram. A significant fraction of the loops has a size larger than 100 nm, exceeding the typical thickness of a TEM foil. Such large loops are often cut off by the foil surface and displayed as bows. Their identification in TEM images was only possible if at least 1/3 of the original circle is visible. The high density of line dislocations in the coarse area is an additional factor affecting the statistics. It can also be assumed that a considerable number of the larger loops were imaged as line dislocations and not detected as loop or "radiation-induced defects".

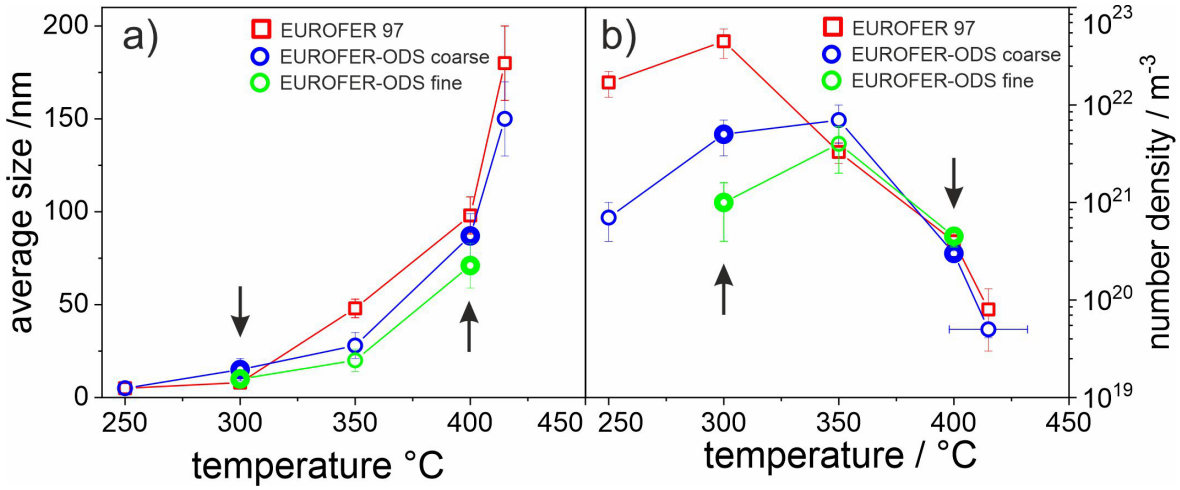

Fig. 11 Dependence of the average size (a) and number density (b) of dislocation loops in EUROFER97 [3] (red squares) and EUROFER-ODS [13] (blue and green circles) on irradiation temperature.

Quantitative data on dislocation loops were compared with EUROFER97 and EUROFER-ODS from the entire SPICE irradiation program [3,12] (Fig.11). The data described in this publication are drawn with a thick symbol and additionally marked with black arrows. The average size and number density from the "fine" range in EUROFER-ODS were both plotted only for 300°C, 350°C, and 400°C (green circles), since the no loops were observed at 250°C and 415°C [12]. The average size of the loops is almost identical for both alloys at 250°C and 300°C, while at higher temperatures it appears systematically ~20-35% smaller in ODS material than in EUROFER97 (Fig. 11a).

The number density of dislocation loops shows a significant difference between both alloys at an irradiation temperature of 250°C and 300°C (Fig. 11b), respectively. Their value is one order of magnitude higher in EUROFER97 than in the "coarse" area of the EUROFER-ODS. However, at higher irradiation temperatures, the number densities of both EUROFER and EUROFER-ODS are comparable. The highest number density was measured for EUROFER-ODS irradiated at 350°C, while for EUROFER97 it reaches its maximum at 300°C. In summary it can be noted that the loops in the "fine" area are systematically smaller in size and have a lower number density than in the "coarse" area. It is assumed that the suppression of radiation damage by the ODS particles is only effective up to 350°C. At higher temperatures, the formation of dislocation loops is fairly independent of their presence and morphology.

The growth of interstitial dislocation loops during irradiation results from the interstitial elastic misfit, which forces dislocations to attract interstitials stronger than vacancies [33]. A dislocation loop is then formed by inserting a circular plane of atoms between closely packed atomic planes. The additional volume introduced this plane is referred to as relaxation volume

the dislocation loop [34]. Accordingly, the relaxation volume Ω can be calculated as the volume of the prism by Ω=b*A expression, where b is the Burgers vector and A is the surface area of the dislocation loop. The values of the Burgers vectors for b½<111> and b<100> loops were calculated as $b_{½<111>} = ½a_0\sqrt{3} = 0.247\ nm$ and $b_{<100>} = a_0 = 0.286\ nm$, respectively.

The diagram plotted in Fig. 12 shows the dependence of the relaxation volume of the interstitial loops in EUROFER97 and EUROFER-ODS on the irradiation temperatures. It is noticeable that the cumulative relaxation volume in EUROFER-ODS is systematically smaller than in EUROFER97, which was irradiated under the same conditions. The maximum value was measured at 350°C for both alloys (Fig. 12, Tab. 3). At temperatures exceeding 400°C, the measurement error increases significantly due to the difficulty in identifying the loops and the uncertainty in size determination. Those loops larger than the thickness of the TEM film are often visible as line dislocations [3]. It should be noticed that information on dislocation loops formed at higher temperatures is scarce. Yao et al. [15] reported loops with sizes exceeding 150 nm in pure single crystal iron after ion irradiation at 500°C. Theoretical studies predict that continuous irradiation causes the structural transition from an ensemble of isolated defects to a microstructure dominated by a dislocation network [35]. The formation of a dense dislocation network in the coarse area was also observed within the present work and in [3]. It was also clearly shown that the formation of loops also occurred at 420°C in EUROFER97 and EUROFER-ODS but they are not always recognized as loops by TEM (Fig. 6b).

The dependence of the Burgers vector of the loops in EUROFER97 and EUROFER-ODS on the irradiation temperature is shown in a diagram in Fig. 13. At 250°C and 300°C irradiation, the ½<111>-loops dominate in both alloys. At higher temperatures, the <100> loops form preferentially in EUROFER97, whose percentage increases to over 80%. The ½<111> loops remain In EUROFER-ODS as the dominant defect type for all higher irradiation temperatures except the highest, i.e., 420°C. The preferential formation of ½<111> loops was also observed in ion-irradiated EUROFER-ODS (T_{irr}=400°C), while in EUROFER97 the majority of loops were of the <111> type [36].

The current results imply that ODS alloys with a higher number density of "fine" nano oxides have a higher radiation resistance than alloys with "coarse" ODS particles and a low number density. The differences between "coarse" and "fine" areas are evident at all irradiation temperatures. At 350°C, the damage reaches a maximum value i.e., increased formation of

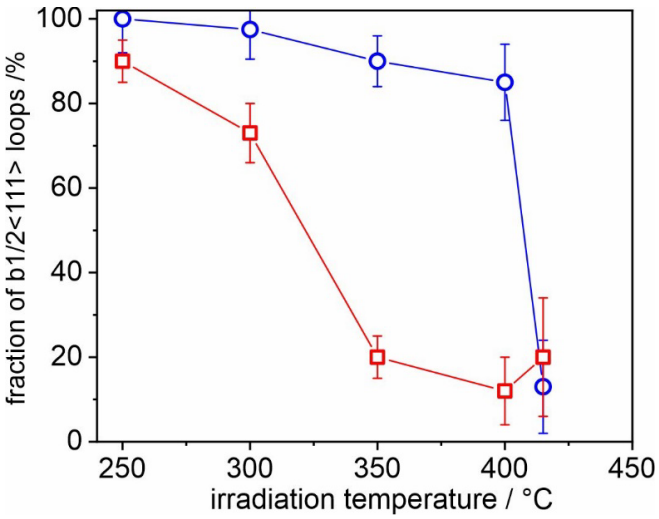

Fig. 13 Dependence of Burgers vector on irradiation temperature for EUROFER97 (red squares) and EUROFER-ODS (blue circles).

voids and dislocation loops (Fig. 11b, Fig. 12). This effect was also observed in boron-alloyed EUROFER97 [32] and other materials irradiated under the similar irradiation conditions [2].

Numerous ODS alloys were developed and fabricated during past decade. The number density of nano-sized particles varied by about two orders of magnitude from ~10^{23} m^{-3} in nanostructured ferritic alloys [22] down to ~10^{21} m^{-3} in ODS alloys of PM2000 type [30] or EUROFER-ODS [12,27]. The presence of highly dispersed oxide particles effectively suppresses the formation of radiation-induced defects and thus minimizes their effect on mechanical properties such as hardening. This has been observed in ferritic-martensitic 9-10Cr ODS steels (such as EUROFER-ODS) and nanoscale ferritic 13-17Cr ODS steels (such as 14YWT) [37,38]. Although this important observation has not yet been analyzed quantitatively in existing literature, e.g., by computational materials science. It now seems qualitatively obvious that radiation-induced loops are unlikely to form while the existing sink force density is exceeding a certain threshold value. This means that, when the number density of nanoscale oxide particles (e.g. Y_2O_3, $Y_2Ti_2O_5$) significantly exceeds the loop number density in conventional particle-free cast steel irradiated under the same conditions. The critical number density of ODS particles is ~10^{22} m^{-3} for an irradiation temperature of 250-300°C. In alloys with higher number density of ODS particles, irradiation-induced Frenkel defects do not contribute with high probability to nucleation and growth of stable loops, but rather are annihilated by trapping at the ODS-particle matrix interface. Homogeneously dispersed, nano oxides have therefore an outstanding additional function: They are not only the foundation for high-temperature creep and fatigue strength but also remarkably reduce irradiation hardening and consequently retard substantially irradiation embrittlement at lower strain rates relevant for tensile and creep experiments.

5. **Conclusions**

The study presents a detailed microstructural examination of neutron irradiated EUROFER–ODS at 300°C and 400°C. This involves imaging of radiation-induced defects under weak beam conditions and their quantitative analysis, which includes determination of their Burger vector, nature, morphology and spatial distribution. The presence of ODS particles inside EUROFER-ODS generally minimize the formation of radiation-induced defects, as shown by comparison with the otherwise identical alloy EUROFER97.The finely dispersed nano oxides with a number density higher than 10^{23} m^{-3} show a significantly stronger effect than larger ODS particles with lower number density. This is particularly the case for irradiation temperatures of 300°C and below. Despite the fact that the highest number density of radiation-induced defects was measured at <300°C, the largest effect on the microstructure, measured by the cumulative volume of dislocation loops, was determined to be at 350°C. The microstructure was found to be dominated by interstitial loops with mainly ½<111> Burgers vector.

The results were supplemented with data from EUROFER-ODS irradiated at other temperatures [12] and compared with EUROFER97 irradiated as the part of the same irradiation campaign [3]. This analysis provides the opportunity to examine the influence of ODS particles on the formation of radiation-induced defects in the temperature range from 250°C to 450°C.

.

6. **Acknowledgements:**

This work has been carried out within the framework of the EUROfusion Consortium and has received funding from the Euratom research and training programme 2014-2018 and 2019-2020 under grant agreement No 633053. The views and opinions expressed herein do not necessarily reflect those of the European Commission.

Figures:

Fig. 1. Fig. 1 Analytical examination of unirradiated EUROFER-ODS. The HAADF image of analyzed area is shown in part (a) and the maps of the corresponding elements imaged with reverse contrast are shown in parts (b-e). Part (c) shows an enlarged section from part (b) which is marked with a square. The part (f) represents composition of Y (red), Ta (blue) and Fe (green) maps.

Fig. 2. Microstructure of EUROFER-ODS irradiated at 300°C. The Y map (b) and Cr (c) maps indicate the location of the “fine” and “coarse” areas as well as $M_{23}C_6$ precipitates.

Fig. 3. The micrographs of the "fine area" obtained at WBDF conditions with selected ***g***-vectors near [111] ZA and imaged with reversal contrast.

Fig. 4. The micrographs of the "coarse area" obtained at WBDF conditions with selected ***g***-vectors near [111] ZA and imaged with reversal contrast.

Fig. 5. Formation of helical dislocations in the “fine area”.

Fig. 6. The BF image of ODS particles with voids (a) and BF image illustrating the distribution of dislocations in the “coarse” (red arrow) and “fine” (blue arrow) areas (b).

Fig. 7. The micrographs obtained at WBDF conditions with selected ***g***-vectors near [100] ZA (parts a-d). The part (e) shows the presence of ***b***<100> loops. In part (f), loops with ***b***[1-11] and ***b***[111] Burgers vectors are schematically drawn with red and blue colors, and ***b***[010] and ***b***[001] loops are drawn with green and yellow colors, respectively.

Fig. 8. The interaction of ***b***½<111> loops imaged with different g-vectors near [100] zone axis. The loops are drawn in part (c) with colors according to the Tab. 2: ***b***½[1-11] red, ***b***½[111] blue, ***b***[002] yellow and ***b***[020] green.

Fig. 9. The micrographs shows a possible interaction of line dislocations with dislocation loops.

Fig. 10. Size distribution histograms of dislocation loops for 300°C and 400°C irradiation temperatures.

Fig. 11 Dependence of average size (a) and number density (b) of dislocation loops in EUROFER-97 [3] (red squares) and EUROFER-ODS [12] (blue and green circles) on irradiation temperature.

Fig. 12 Relaxation volume of interstitial dislocation loops formed in EUROFER97 and EUROFER-ODS as a function of radiation temperature.

Fig. 13 Dependence of Burgers vector on irradiation temperature for EUROFER97 (red squares) and EUROFER-ODS (blue circles).

References

[1] J. Knaster, A. Moeslang, T. Muroga, Materials research for fusion, Nature Phys 12 (2016) 424–434. https://doi.org/10.1038/nphys3735.

[2] A. Kimura, Current Status of Reduced-Activation Ferritic/Martensitic Steels R&D for Fusion Energy, Mater. Trans. 46 (2005) 394–404. https://doi.org/10.2320/MATERTRANS.46.394.

[3] M. Klimenkov, U. Jäntsch, M. Rieth, A. Möslang, Correlation of microstructural and mechanical properties of neutron irradiated EUROFER97 steel, Journal of Nuclear Materials 538 (2020) 152231. https://doi.org/10.1016/j.jnucmat.2020.152231.

[4] E. Aydogan, J.S. Weaver, U. Carvajal-Nunez, M.M. Schneider, J.G. Gigax, D.L. Krumwiede, P. Hosemann, T.A. Saleh, N.A. Mara, D.T. Hoelzer, B. Hilton, S.A.

Maloy, Response of 14YWT alloys under neutron irradiation: A complementary study on microstructure and mechanical properties, Acta Materialia 167 (2019) 181–196. https://doi.org/10.1016/j.actamat.2019.01.041.
[5] J. Wang, M.B. Toloczko, V.N. Voyevodin, V.V. Bryk, O.V. Borodin, V.V. Mel'nychenko, A.S. Kalchenko, F.A. Garner, L. Shao, Atom probe tomography characterization of high-dose ion irradiated MA957, Journal of Nuclear Materials 545 (2021) 152528. https://doi.org/10.1016/j.jnucmat.2020.152528.
[6] T. Gräning, M. Klimenkov, M. Rieth, C. Heintze, A. Möslang, Long-term stability of the microstructure of austenitic ODS steel rods produced with a carbon-containing process control agent, Journal of Nuclear Materials 523 (2019) 111–120. https://doi.org/10.1016/j.jnucmat.2019.05.060.
[7] S. Chen, Y. Wang, K. Tadaki, N. Hashimoto, S. Ohnuki, Suppression effect of nano-sized oxide particles on helium irradiation hardening in F82H-ODS steel, Journal of Nuclear Materials 455 (2014) 301–305. https://doi.org/10.1016/j.jnucmat.2014.06.041.
[8] M. Kolluri, P.D. Edmondson, N.V. Luzginova, F. Berg, A structure–property correlation study of neutron irradiation induced damage in EU batch of ODS Eurofer97 steel, Materials Science and Engineering: A 597 (2014) 111–116. https://doi.org/10.1016/j.msea.2013.12.074.
[9] C. Heintze, F. Bergner, M. Hernández-Mayoral, R. Kögler, G. Müller, A. Ulbricht, Irradiation hardening of Fe–9Cr-based alloys and ODS Eurofer: Effect of helium implantation and iron-ion irradiation at 300 °C including sequence effects, Journal of Nuclear Materials 470 (2016) 258–267. https://doi.org/10.1016/j.jnucmat.2015.12.041.
[10] A.I. Ryazanov, O.K. Chugunov, S.M. Ivanov, S.T. Latushkin, R. Lindau, A. Möslang, A.A. Nikitina, K.E. Prikhodko, E.V. Semenov, V.N. Unezhev, P.V. Vladimirov, Tensile properties and microstructure of helium implanted EUROFER ODS, Journal of Nuclear Materials 442 (2013) S153-S157. https://doi.org/10.1016/j.jnucmat.2013.03.080.
[11] J.P. Wharry, M.J. Swenson, K.H. Yano, A review of the irradiation evolution of dispersed oxide nanoparticles in the b.c.c. Fe-Cr system: Current understanding and future directions, Journal of Nuclear Materials 486 (2017) 11–20. https://doi.org/10.1016/j.jnucmat.2017.01.009.
[12] M. Klimenkov, R. Lindau, U. Jäntsch, A. Möslang, Effect of irradiation temperature on microstructure of ferritic-martensitic ODS steel, Journal of Nuclear Materials 493 (2017) 426–435. https://doi.org/10.1016/j.jnucmat.2017.06.024.
[13] E. Materna-Morris, R. Lindau, H.-C. Schneider, A. Möslang, Tensile behavior of EUROFER ODS steel after neutron irradiation up to 16.3 dpa between 250 and 450 °C, Fusion Engineering and Design 98-99 (2015) 2038–2041. https://doi.org/10.1016/j.fusengdes.2015.07.015.
[14] N. Akasaka, S. Yamashita, T. Yoshitake, S. Ukai, A. Kimura, Microstructural changes of neutron irradiated ODS ferritic and martensitic steels, Journal of Nuclear Materials 329-333 (2004) 1053–1056. https://doi.org/10.1016/j.jnucmat.2004.04.133.
[15] Z. Yao, M.L. Jenkins, M. Hernández-Mayoral, M.A. Kirk, The temperature dependence of heavy-ion damage in iron: A microstructural transition at elevated temperatures, Philosophical Magazine 90 (2010) 4623–4634. https://doi.org/10.1080/14786430903430981.
[16] H.J. Jung, D.J. Edwards, R.J. Kurtz, T. Yamamoto, Y. Wu, G.R. Odette, Structural and chemical evolution in neutron irradiated and helium-injected ferritic ODS PM2000 alloy, Journal of Nuclear Materials 484 (2017) 68–80. https://doi.org/10.1016/j.jnucmat.2016.11.022.
[17] N. Baluc, R. Schäublin, P. Spätig, M. Victoria, On the potentiality of using ferritic/martensitic steels as structural materials for fusion reactors, Nucl. Fusion 44 (2004) 56–61. https://doi.org/10.1088/0029-5515/44/1/006.

[18] E. Materna-Morris, A. Möslang, H.-C. Schneider, Tensile and low cycle fatigue properties of EUROFER97-steel after 16.3dpa neutron irradiation at 523, 623 and 723K, Journal of Nuclear Materials 442 (2013) S62-S66. https://doi.org/10.1016/j.jnucmat.2013.03.038.
[19] M. Klimiankou, R. Lindau, A. Möslang, Direct correlation between morphology of (Fe,Cr)23C6 precipitates and impact behavior of ODS steels, Journal of Nuclear Materials 367-370 (2007) 173–178. https://doi.org/10.1016/j.jnucmat.2007.03.150.
[20] R. Schaeublin, T. Leguey, P. Spätig, N. Baluc, M. Victoria, Microstructure and mechanical properties of two ODS ferritic/martensitic steels, Journal of Nuclear Materials 307-311 (2002) 778–782. https://doi.org/10.1016/S0022-3115(02)01193-5.
[21] R. Lindau, M. Klimenkov, U. Jäntsch, A. Möslang, L. Commin, Mechanical and microstructural characterization of electron beam welded reduced activation oxide dispersion strengthened – Eurofer steel, Journal of Nuclear Materials 416 (2011) 22–29. https://doi.org/10.1016/j.jnucmat.2011.01.025.
[22] G.R. Odette, Recent Progress in Developing and Qualifying Nanostructured Ferritic Alloys for Advanced Fission and Fusion Applications, JOM 66 (2014) 2427–2441. https://doi.org/10.1007/s11837-014-1207-5.
[23] M. Klimenkov, A. Möslang, R. Lindau, EELS analysis of complex precipitates in PM 2000 steel, Eur. Phys. J. Appl. Phys. 42 (2008) 293–303. https://doi.org/10.1051/EPJAP:2008084.
[24] C. Eiselt, M. Klimenkov, R. Lindau, A. Möslang, H. Sandim, A.F. Padilha, D. Raabe, High-resolution transmission electron microscopy and electron backscatter diffraction in nanoscaled ferritic and ferritic–martensitic oxide dispersion strengthened–steels, Journal of Nuclear Materials 385 (2009) 231–235. https://doi.org/10.1016/j.jnucmat.2008.11.029.
[25] P. He, M. Klimenkov, R. Lindau, A. Möslang, Characterization of precipitates in nano structured 14% Cr ODS alloys for fusion application, Journal of Nuclear Materials 428 (2012) 131–138. https://doi.org/10.1016/j.jnucmat.2011.08.026.
[26] M. Stricker, D. Weygand, Dislocation multiplication mechanisms – Glissile junctions and their role on the plastic deformation at the microscale, Acta Materialia 99 (2015) 130–139. https://doi.org/10.1016/j.actamat.2015.07.073.
[27] R. Schäublin, A. Ramar, N. Baluc, V. de Castro, M.A. Monge, T. Leguey, N. Schmid, C. Bonjour, Microstructural development under irradiation in European ODS ferritic/martensitic steels, Journal of Nuclear Materials 351 (2006) 247–260. https://doi.org/10.1016/j.jnucmat.2006.02.005.
[28] S. Rogozhkin, A. Bogachev, O. Korchuganova, A. Nikitin, N. Orlov, A. Aleev, A. Zaluzhnyi, M. Kozodaev, T. Kulevoy, B. Chalykh, R. Lindau, J. Hoffmann, A. Möslang, P. Vladimirov, M. Klimenkov, M. Heilmaier, J. Wagner, S. Seils, Nanostructure evolution in ODS steels under ion irradiation, Nuclear Materials and Energy 9 (2016) 66–74. https://doi.org/10.1016/j.nme.2016.06.011.
[29] M.J. Swenson, J.P. Wharry, The comparison of microstructure and nanocluster evolution in proton and neutron irradiated Fe–9%Cr ODS steel to 3 dpa at 500 °C, Journal of Nuclear Materials 467 (2015) 97–112. https://doi.org/10.1016/j.jnucmat.2015.09.022.
[30] M. Klimiankou, R. Lindau, A. Möslang, Energy-filtered TEM imaging and EELS study of ODS particles and argon-filled cavities in ferritic-martensitic steels, Micron (Oxford, England 1993) 36 (2005) 1–8. https://doi.org/10.1016/j.micron.2004.08.001.
[31] N. Zimber, P. Vladimirov, M. Klimenkov, U. Jäntsch, R. Vila, V. Chakin, F. Mota, Microstructural evolution of three potential fusion candidate steels under ion-irradiation, Journal of Nuclear Materials 535 (2020) 152160. https://doi.org/10.1016/j.jnucmat.2020.152160.

[32] M. Klimenkov, A. Möslang, E. Materna-Morris, Helium influence on the microstructure and swelling of 9%Cr ferritic steel after neutron irradiation to 16.3 dpa, Journal of Nuclear Materials 453 (2014) 54–59. https://doi.org/10.1016/j.jnucmat.2014.05.001.
[33] N.A. Smallman R.E., Modern Physical Metallurgy, Elsevier, 2014.
[34] S.L. Dudarev, P.-W. Ma, Elastic fields, dipole tensors, and interaction between self-interstitial atom defects in bcc transition metals, Phys. Rev. Materials 2 (2018). https://doi.org/10.1103/PhysRevMaterials.2.033602.
[35] P.M. Derlet, S.L. Dudarev, Microscopic structure of a heavily irradiated material, Phys. Rev. Materials 4 (2020). https://doi.org/10.1103/PhysRevMaterials.4.023605.
[36] D. Brimbal, L. Beck, O. Troeber, E. Gaganidze, P. Trocellier, J. Aktaa, R. Lindau, Microstructural characterization of Eurofer-97 and Eurofer-ODS steels before and after multi-beam ion irradiations at JANNUS Saclay facility, Journal of Nuclear Materials 465 (2015) 236–244. https://doi.org/10.1016/j.jnucmat.2015.05.045.
[37] D.A. McClintock, M.A. Sokolov, D.T. Hoelzer, R.K. Nanstad, Mechanical properties of irradiated ODS-EUROFER and nanocluster strengthened 14YWT, Journal of Nuclear Materials 392 (2009) 353–359. https://doi.org/10.1016/j.jnucmat.2009.03.024.
[38] S.J. Zinkle, A. Möslang, T. Muroga, H. Tanigawa, Multimodal options for materials research to advance the basis for fusion energy in the ITER era, Nucl. Fusion 53 (2013) 104024. https://doi.org/10.1088/0029-5515/53/10/104024.